Electron Tunneling Paths in Proteins

Author(s): Atsuo Kuki and Peter G. Wolynes

Source: *Science*, Jun. 26, 1987, New Series, Vol. 236, No. 4809 (Jun. 26, 1987), pp. 1647-1652

Published by: American Association for the Advancement of Science

Stable URL: http://www.jstor.com/stable/1699319

Electron Tunneling Paths in Proteins

ATSUO KUKI* AND PETER G. WOLYNES

One of the crucial issues in biological electron transfer is the determination of the role of spatially intermediate amino acid residues in controlling or directing the electronic tunneling interaction between redox sites. A quantum path integral Monte Carlo method is developed for the analysis of electronic tunneling pathways in a highly structured environment. This path integral method is applied to intramolecular electron transfer in a ruthenium-modified myoglobin that contains a tryptophan in the "line-of-flight." A principal result is the identification of the relevant cylindrical zone swept out by the tunneling electron.

THE LONG-RANGE TRANSFER OF ELECTRONS THAT OCCURS in many important biological systems is a process with inherently quantum mechanical aspects. The dynamics of such reactions depends on both the tunneling of the electrons and the nuclear rearrangements of the protein itself (*1*). The nuclear motion often can be regarded as being nearly classical, but the electronic motion requires a fully quantum mechanical treatment. The quantum nature of the electronic motion blurs many of the issues that chemists seek to confront in biological electron transfer. Foremost is the question of the role of the intervening protein in modifying the rate of electron transfer. Simple quantum mechanical models treat the protein as a structureless medium (*2*) and predict a simple exponential distance dependence of the electron transfer rate. However, the protein clearly has a detailed structure and specific features of this structure may control or facilitate the electron tunneling. There has been much speculation about this. For example, certain residues that are evolutionarily conserved are thought to be essential in accelerating the electron transfer rate in cytochromes (*3*). Gray and co-workers have studied the distance dependence of electron transfer rates in chemically modified myoglobins [penta-amineruthenium-modified zinc myoglobins, a_5RuMb(ZnP), where a is NH_3 and Mb is myoglobin] (*4*). The anomalously higher rate in one case may indicate that a tryptophan is accelerating this process. The recent elucidation of the structure of the photosynthetic reaction center has also spurred speculation on this issue. Further experiments based on site-directed mutagenesis should be helpful in settling some of these issues (*5*).

From the theoretical side, the quantitative analysis of the part played by individual residues in the protein requires some definition of the meaning of an electron transfer path. In this research article we illustrate how Feynman's path integral formulation of quantum mechanics can be used to make the idea of electron transfer paths in proteins more meaningful. The use of path integral ideas in describing tunneling processes is not new; these ideas have been used in many areas of chemistry and physics. For simple problems in gas-phase dynamics, semiclassical descriptions of tunneling paths have been presented (*6, 7*), as have equivalent ideas in quantum field theory both for particle physics (*8*) and applications in condensed matter physics (*9*). In those fields the picturesque terminology of "instanton" or "soliton" is used to describe tunneling paths. The implementation of these ideas in the biomolecular context requires some new tools. First, the electron transfer process is a many-electron problem. The problem is reduced to a one-electron description by means of pseudopotentials (*10*). Second, the heterogeneous structure of the protein and its concomitantly complicated energy surface for electron motion requires computational techniques that do not limit one a priori to a semiclassical description of the tunneling. Therefore we use a Monte Carlo approach to evaluate path integrals and, at the same time, as a search procedure for tunneling paths. Our computational scheme also allows us to define a "linear action relationship" that quantifies the influence of an individual part of the protein on the transfer rate. These linear action relationships are apt to be valid regardless of the details of our specific model.

Basic electron transfer theory. A reasonable starting point for the analysis of an electron transfer reaction is the two-surface Born-Oppenheimer (BO) approximation. The actual motion of the electrons is sufficiently rapid so that in comparison the nuclei can be considered fixed. For extremely long-range transfer the transit time of the electron may be comparable to the time scale of nuclear motion and thus deviations from the two-surface BO picture may become important (*11*). We do not consider this effect here. In the two-surface BO picture nuclear motion takes place on an electronic energy surface that corresponds either to the "neutral" configuration DA or to the "ionic" potential energy surface D^+A^-. If electron tunneling were disallowed, these two electronic states would not communicate. Nevertheless, the tunneling does couple these states through a tunneling matrix element Δ that gives the probability amplitude for transitions between the surfaces at fixed nuclear configuration. If Δ is sufficiently small, second-order perturbation theory (the "Golden Rule") gives an expression for the rate of transition between the two electronic states as a thermal average of the rate between two particular nuclear-motion eigenstates on each of the two potential energy surfaces:

$$k_{ET} = (2\pi/\hbar) \langle |H_{if}|^2 \rho_f(E_i) \rangle \quad (1)$$

where H_{if} is the perturbation matrix element between the initial and final vibronic states and $\rho_f(E_i)$ is the density of final states at the initial energy E_i (*12*). For our model, H_{if} is proportional to Δ and to the overlap matrix element between the initial and final vibrational states (the Franck-Condon factor). Thus the rate depends on the electronic dynamics only through the square of the tunneling matrix

The authors are from the Noyes Laboratory, University of Illinois, Urbana, IL 61801.

*Current address: Baker Laboratory, Cornell University, Ithaca, NY 14853.

element. Ideally the nuclear motion factors can be eliminated by considering a series of reactions in which the donor and acceptor have a nearly constant local environment but have a varying spatial relation to each other. This is the goal of the strategy used by Gray and co-workers in their experiments (*4*).

An alternative view of the electron transfer process is provided by the surface-hopping picture. If the nuclear motion is considered to be classical, the critical configuration in the rate process is at the crossing of the two potential energy surfaces. It is only in the vicinity of this crossing surface where the resonance condition can be satisfied and the electron can hop. Again, for small Δ, the probability of making a hop is proportional to Δ^2. The thermal average in the Golden Rule expression (Eq. 1) essentially gives the same result as that from the surface-hopping picture. The hopping picture is especially convenient for understanding the breakdown of the Golden Rule result that occurs for large Δ. Frauenfelder and Wolynes give a didactic discussion of this issue in the context of biomolecular reactions (*13*). The hopping picture makes clear that the Δ evaluated at those nuclear configurations which are isoenergetic as DA or D^+A^- is the crucial value in determining the rate. This fact makes possible the determination of the relevant Δ by path integral methods.

Path integral analysis of tunneling. Although tunneling is a dynamic process that determines reaction rates, it is mathematically convenient to analyze the thermodynamic consequences of tunneling. The tunneling process causes a splitting between the adiabatic potential surfaces so that they are never truly degenerate. This splitting is 2Δ at the crossing point of the zeroth-order surfaces; Δ can be determined by examination of the thermal off-diagonal electronic density matrix at the crossing point. Alternatively, a similar but less computationally convenient approach is provided by considering imaginary time flux correlation functions for the electron followed by analytic continuation to real time (*14*,*15*). The off-diagonal electronic density matrix between two states, 1 and 2, is determined by an imaginary time propagation $G_{12} = \langle 1|e^{-\beta H}|2\rangle$, where β is the inverse thermal energy $[(k_B T)^{-1}$, where k_B is Boltzmann's constant] and H is the Hamiltonian for the system. This propagator can be represented as a path integral:

$$\langle 1|e^{-\beta H}|2\rangle = \int dx_i\, \psi_1(x_i) \int dx_f\, \psi_2(x_f) \int \mathcal{D}x(\beta)\, \exp\left\{-\int_0^\beta H(x(\beta'))\, d\beta'\right\} \quad (2)$$

where

$$H(x(\beta)) = \frac{m}{2}\left(\frac{dx}{d\beta}\right)^2 + V(x(\beta)) \quad (3)$$

and $V(x)$ is the potential on which the electron moves with path $x(\beta')$. The $\mathcal{D}$ symbols indicate path integration; x_i and x_f are coordinates for the initial and final states, respectively, and m is the mass of the electron. The integral from 0 to β of $H(x(\beta'))\, d\beta'$ is the action for imaginary time motion. In our case $V(x)$ consists of (i) the sum of pseudopotentials that describe an electron moving around each of the atoms in the protein and of (ii) two wells that describe the electron when it is bound in the donor or the acceptor. To determine Δ we choose ψ_1 to be a wave function that is localized on the donor and ψ_2 to be a wave function that is localized on the acceptor. The detailed choice of ψ_1 and ψ_2 is immaterial provided that they overlap strongly with the actual states involved in the reaction. The path sum in Eq. 2 is isomorphic to that of a flexible polymer that interacts with the external potential $V(x)$. This analogy can be made more explicit by considering a discrete approximation to the path integral (*7*). If the path is cut up into P segments we can write the path integral as:

$$\int_{x_i}^{x_f} \mathcal{D}x \exp\left\{-\int_0^\beta H(x(\beta'))\, d\beta'\right\} = \int dx_1 \int dx_2 \cdots \int dx_{P-1} \left(\frac{m}{2\pi\hbar^2\beta/P}\right)^{3P/2} \times \exp\left[-\left(\frac{\beta}{P}\right)\sum_i \frac{m(x_i - x_{i-1})^2}{2\hbar^2\,(\beta/P)^2} + V(x_i)\right] \quad (4)$$

Thus the kinetic energy in Eq. 3 has been translated into the potential energy of harmonic springs that connect neighboring points in the isomorphic polymer chain. This discrete version of the path sum is particularly suggestive of both physical analogies and computational procedures. Exact results require taking the limit $P \to \infty$, but the finite P approximation can be used for numerical computation.

The analysis of tunneling in a multistable potential relies on a classification of the paths that contribute to the path integral in Eq. 2 (*7*, *8*). Consider the total imaginary time β to be very long. That is, we take $\beta\Delta E >> 1$, where ΔE is the excitation energy from the quasi-degenerate levels to the third lowest level. In this case a typical path that contributes to Eq. 2 is in well A for a relatively long period of time before rapidly making a transit to well B, where it resides again for a relatively long period of time. We will call such a rapid transit a "kink." Other paths that contribute to the path sum will have a larger but odd number of such kinks. Typically the kinks will be well separated in time and can be considered to be noninteracting. The excursion represented by such a kink is costly in energy; however, if β is large, multikink configurations are favored because of their large number. The free energy of introducing a kink is F_k and is the difference between the free energy of a one-kink path and that of a path of equivalent β that is confined to one well, E_0 (since the wells are isoenergetic at the crossing point, it does not matter which one). The path sum can be written as an expansion in kinks. The contributions of paths with N kinks to the path sum is

$$(1/N!)e^{-N\beta F_k}\, e^{-\beta E_0} \quad (5)$$

if the interaction between kinks can be neglected. In this expression F_k includes the integration over the position of the center of the kink, and the factor of $1/N!$ arises from the indistinguishability of the kinks. Thus one finds that the amplitude for a transition from state 1 to state 2 can be represented as the sum

$$e^{-\beta E_0} \sum_{N\ \text{odd}} (1/N!)e^{-N\beta F_k} = e^{-\beta E_0} \sinh(e^{-\beta F_k}) \quad (6)$$

This should be compared with the result from ordinary quantum mechanics. If there are two quasi-degenerate states with the energies $E_0 \pm \Delta$, then the same amplitude can be written as $e^{-\beta E_0} \sinh(\beta\Delta)$. Upon analytic continuation to real time the hyperbolic sine becomes the oscillatory circular sine function, which is the well-known Rabi oscillation of a two-level system. Thus the tunneling amplitude is exponentially related to the free energy of introducing a kink:

$$\Delta = (1/\beta)\, e^{-\beta F_k} \quad (7)$$

This free energy in turn can be obtained by looking at configurations with only a single transit from donor to acceptor well. The Δ thus obtained is independent of the β used in the calculation.

In semiclassical theories of tunneling additional approximations are made to determine F_k. In these theories an extremal one kink

path is found. If we extremize the action $H(x(\beta))$ we obtain the imaginary time classical equations of motion. The free energy F_k will be the action associated with such an extremal path plus a contribution from the small amplitude oscillations about this path, which are treated harmonically.

The semiclassical argument easily gives the expected exponential behavior of Δ as a function of distance r when the protein is treated as a featureless flat potential. Classical motion in a flat potential is rectilinear. The extremal path is therefore the minimum distance straight line from well A to well B. The action of a straight-line path is proportional to its length and thereby gives Δ proportional to e^{-r/r_0}, where r_0 is the minimum distance between wells.

For the complicated potential provided by the protein it is not obvious a priori that the semiclassical approach will work. Multiple classical paths may result from the scattering of the electron by intermediate residues. The harmonic treatment of the small amplitude fluctuations about the classical paths is also suspect because of the rapidly varying nature of the electron-atom pseudopotentials. Thus alternative routes to the kink free energy are needed. A very instructive route is provided by Monte Carlo calculations. Monte Carlo methods evaluate high-dimensional integrals by the application of probabilistic sampling (*16*) and thus can be used to evaluate the path integral expression for the tunneling matrix element. To complete the connection some thermodynamic manipulation is required.

One Monte Carlo procedure is to sample the paths according to the weight in Eq. 4 by using Metropolis sampling (*17*). This procedure gives information about which paths are important. Thus we can use it as a search procedure to find classical paths, as in simulated annealing (*18*). Furthermore, the density of paths at intermediate positions gives information on the importance of those intermediate regions in determining the matrix element. If a large density of points accumulates on an intermediate amino acid residue, that residue should be thought of as enhancing the tunneling interaction. However, this straightforward Monte Carlo sampling does not directly give free energies, as they are not averages of a mechanical quantity.

The free energy involved in computing the tunneling can be computed in a series of steps that resemble a thermodynamic cycle. We start with a potential $V_0(x)$ for which we know the kink free energy exactly. A set of simple spherical well potentials is usually chosen. Then we slowly change this reference potential to the full potential $V(x)$ in steps by performing Monte Carlo calculations with the potential $V_0(x) + \lambda[V(x)-V_0(x)]$, where $0 < \lambda < 1$. The free energy can be computed in two ways. If a small change in λ is made we can write

$$\left.\frac{\partial F}{\partial \lambda}\right|_\lambda = \left\langle \frac{1}{P}\sum_i V(x_i) - V_0(x_i) \right\rangle_\lambda \tag{8}$$

where the average is taken in the partially changed system for a path configuration with one kink. Thus we can compute the change in the tunneling matrix element by using a series of Monte Carlo runs at intermediate values of λ

$$\ln(\Delta/\Delta_0) = -\beta\,[F(\lambda = 1) - F(\lambda = 0)]$$

$$= -\beta\int_0^1 d\lambda\,\frac{\partial F}{\partial \lambda} =$$

$$-\beta\int_\lambda^1 d\lambda\,\left\langle \frac{1}{P}\sum_i V(x_i) - V_0(x_i) \right\rangle_\lambda \tag{9}$$

This procedure works reasonably well if $V(x)$ is fairly smooth. If $V(x)$ is harshly repulsive a different approach introduced by Widom for hard-sphere fluids can be used (*19*). If a small but discrete change in λ is made the ratio of tunneling matrix elements can be found by averaging the change in Boltzmann factors of a path in the unperturbed ensemble:

$$\Delta(\lambda_2)/\Delta(\lambda_1) = \langle \exp\,[-(\lambda_2 - \lambda_1)(\beta/P)\sum_i V(x_i)]\,\rangle_{\lambda_1} \tag{10}$$

We used a combination of these two calculational schemes in our studies.

This approach can be extended particularly when only a few amino acid residues are changed. If only a limited region of the protein is slightly changed we can compute the change in tunneling by functional differentiation

$$\ln\,(\Delta_2/\Delta_1) \cong -\beta\int \frac{\delta F}{\delta V(r)}\,[V_2(r) - V_1(r)]\,d^3r \tag{11}$$

Standard statistical mechanical reasoning gives

$$\frac{\delta F}{\delta V(r)} = \rho_{\text{kink}}(r) \tag{12}$$

where $\rho_{\text{kink}}(r)$ is the density of electron paths in a kink at the point r, which is computed in the ensemble with potential V_1. This electron density can be computed directly in a Monte Carlo simulation.

An important relation is suggested by Eq. 12 that can be easily tested experimentally through site-directed mutagenesis. If a local change in V is made, then the right-hand side of Eq. 12 is roughly a product of a protein-dependent factor $\rho_{\text{kink}}(r)$ and an amino acid residue–dependent factor. The amino acid residue–dependent factor should also depend on the electron affinity of the amino acid. Thus a plot of log Δ (or log k_{ET}) versus electron affinity should give a straight line whose slope reflects the density of electron paths at that site. This linear action relationship is a quantum mechanical analog of the linear free energy relationships used for thermally activated processes in chemical kinetics (*20, 21*). The free energy here is that of the classical polymer chain that is isomorphic to the tunneling paths. If electron transfer is through hole states a similar relation with ionization potentials is to be expected.

Pseudopotential for excess electron in protein. Atom-atom potentials that are required in molecular dynamics simulations of proteins (*22*) have been extensively studied. Much less is known about the potential energy of an excess electron in the interior of a protein. We have adapted various pseudopotential approaches from electron-molecule scattering and solvated electron studies as outlined below.

The relevant virtual states of the intervening medium may be excess electron states or hole states. These two superexchange mechanisms require different pseudopotentials. In particular, site-to-site hopping is the more appropriate framework for a calculation of hole tunneling, whereas the local potential described below is suitable for the motion of an excess electron. In a given electron transfer system, the importance of hole compared to electron superexchange is determined by the redox potential of the donor acceptor system at the transition state configuration where DA and D^+A^- are isoenergetic. In the specific protein we have treated, a_5RuMb(ZnP) (*4*), the reorganization energy results mainly from the nuclear motion around the ruthenium site rather than around the porphyrin site, and hence the transition state redox potential is close to that for the porphyrin site. The zinc protoporphyrin reacts from its triplet state which lies 1.8 eV above the ground state and is a potent reductant. Accordingly, our pseudopotential, which describes excess electron states, is a reasonable choice. A full many-electron calculation would have to include the complexity of fermion

statistics (*7*), but such a procedure would avoid this ambiguity.

The closed-shell electron density on each atom of atomic number z is modeled by spherically symmetric exponential wave function ψ_c that generates a potential featuring a repulsive core and an attractive annular region:

$$\psi_c(r) = (z\gamma^3/8\pi)^{\frac{1}{2}} e^{-\gamma r/2}$$

$$V = \sum_{\text{atoms}} V_{\text{charge}} + V_{\text{pol}} + V_{\text{coul}} + V_{\text{ex}}^{\text{NL}} + V_{\text{r}}^{\text{NL}} \qquad (13)$$

The core size parameter γ is inversely proportional to the van der Waals radius r_{vdw} for the particular atom and the proportionality constant was set by fitting γ to the total electron density from Hartree-Fock atomic wave functions. For an aliphatic CH_2 or aromatic CH group, $r_{\text{vdw}} = 1.90$ Å and $\gamma = 5.01$ Å^{-1}. The long-range terms V_{charge} and V_{pol} arise from the net partial charge and polarizabilities of each atom, respectively; these parameters are taken directly from the atom-atom potentials. The divergence of V_{pol} at short range is removed by replacing r^{-4} by $(r^2 + r_{\text{vdw}}^2)^{-2}$. A screening correction that consists of a Lorentz local field factor of 2 (*23*) is applied at radii greater than 3 Å. Penetration into the existing core electron density $|\psi_c|^2$ results in a simple analytic γ-dependent attractive coulomb potential V_{coul} (*24*).

The potentials $V_{\text{ex}}^{\text{NL}}$ and V_{r}^{NL} are the Hartree-Fock exchange term and repulsive pseudopotentials, respectively, and are nonlocal in character (*10*). For ease of implementation of the path integral method, we converted $V_{\text{ex}}^{\text{NL}}$ and V_{r}^{NL} into local potentials (*25*) and calibrated the resulting total potential V against known results in two model cases. A single parameter c that had the same value for all the atoms was introduced in V_{r} and adjusted to yield the correct balance of attractive and repulsive terms as determined by the calibration.

$$V_{\text{ex}} = \frac{V_{\text{ex}}^{\text{NL}}\,\psi_{\text{loc}}}{\psi_{\text{loc}}} = \left(\frac{1}{2}\right)\frac{\psi_c(r)}{\psi_{\text{loc}}(r)}\int \frac{\psi_c(r')\,\psi_{\text{loc}}(r')}{|r - r'|}\,dr' \qquad (14)$$

$$V_{\text{r}} = \frac{-\tilde{P}_c(\tilde{V}_{\text{coul}} + \tilde{V}_{\text{ex}}^{\text{NL}})\,\psi_{\text{loc}}}{\psi_{\text{loc}}}$$

$$= \frac{\bar{\psi}_c(r)}{\psi_{\text{loc}}(r)}\left[\frac{z}{2}\int \frac{\bar{\psi}_c(r')\psi_{\text{loc}}(r')}{r'}\,dr'\right.$$

$$\left. -\frac{1}{4}\int\int \frac{\bar{\psi}_c(r')\,\psi_{\text{loc}}(r')\,\bar{\psi}_c(r'')\,\bar{\psi}_c(r'')}{|r' - r''|}\,dr'\,dr''\right] \qquad (15)$$

$$\bar{\psi}_c(r) = (zc^3\gamma^3/8\pi)^{\frac{1}{2}} e^{-c\gamma r/2} \qquad (16)$$

The local wave function ψ_{loc} describes the penetration of the excess electron into the closed shell of an atom. In this region the electron interacts to a good approximation with that one atom only and a spherically symmetric tunneling form $\psi_{\text{loc}} = [\sinh(kr)]/kr$ is used ($k = 2$ in atomic units) (*24*). The first integral on the right-hand side of Eq. 15 arises from the nuclear attraction term in V_{coul}; the second integral arises from the electron-electron repulsion term in V_{coul} and from the V_{ex} term.

The repulsive pseudopotential term accounts for the Pauli exclusion principle but is controlled by same overall exponential form ψ_c, as are the attractive V_c and V_{ex} terms. Indeed, in the core there is a delicate cancellation between any repulsive pseudopotential and the attractive terms (*26*). Thus it was necessary to include a compression factor $c > 1$ into the wave function ψ_c that was used in the V_{r} computation to satisfy the basic requirement that the repulsive core term rise more steeply than the attractive terms fall. This adjustable parameter c is included in the projector P_c onto the core orbitals. Calculation of the scattering length for electron-neon scattering without polarization provided the calibration for the repulsive core. The Hartree-Fock scattering length is 0.556 Å (*27*) and is matched exactly by our potential for $c = 1.534$. The balance between repulsive core and attractive annular shell interactions was calibrated by the calculation of the energy of a quasi-free electron in benzene, V_0. The experimental value is $V_0 = -0.14$ eV (*28*). By using our potential an estimate for $V_0 = \langle\psi_j|\,H\,|\psi_j\rangle\,/\,\langle\psi_j|\psi_j\rangle$ was obtained by Monte Carlo evaluation of the kinetic and potential energy integrals with uniform sampling for the crystal structure of benzene expanded to match the density of liquid benzene at 25°C. A Jastrow form trial wave function ψ_j for the quasi-free electron was formed as a product of the exact numerical wave functions obtained from the spherical potential of individual aromatic CH extended atoms. At a value of $c = 1.534$ an excessively attractive potential resulted, and the compromise value of $c = 1.5$ was selected, which yielded $V_0 = -0.482$ eV and an electron-neon scattering length of 0.651 Å. It will be significant in view of the results of the protein calculation that our V_0 is more stable and attractive than the experimental value in the benzene calculation. The final aromatic CH extended atom potential has a minimum of -0.90 eV at 1.6 Å and crosses zero at 1.27 Å. The potential for a CH_2 alkyl group has a minimum of -0.61 eV at 1.8 Å and crosses zero at 1.45 Å; the V_0 computed for a simple model of liquid cyclohexane was $+0.069$ eV. While potentials based on more detailed core wave functions than the simple exponential form can be generated by the same procedure (Eq. 13), we feel that our semiempirical pseudopotential captures the essential balance of repulsive and attractive regions around each atom. We retain the full complexity of the protein architecture by including in the potential field for the excess electron all the 1217 nonhydrogen atoms present in myoglobin. As a result of the gradations in the partial charge that arise from the standard adjustments for the surrounding dielectric aqueous medium (*29*), the potential due to each of the 1217 atoms is different.

Metropolis Monte Carlo sampling. The relation between the tunneling splitting and the free energy for the isomorphic one-kink polymer chain (Eq. 7) was tested in a one-dimensional potential composed of two square wells separated by a barrier 9 Å long and 4 eV high. One end of a 128-segment polymer chain was fixed to the center of each square well and the effect upon the tunneling splitting of introducing a third shallow well in the center of the barrier was determined by the integration method of Eq. 9. When $\beta\hbar = 6$ femtoseconds (fsec) the Monte Carlo result for the ratio of three-well to two-well tunneling splittings was 1.56 ± 0.015. With $\beta\hbar = 18$ fsec the Monte Carlo result 1.57 ± 0.02 was obtained. The exact ratio for the two potentials is 1.55979. This demonstrates both the accuracy of the method and the validity of the analysis that the Δ obtained are independent of the value of β employed.

For the protein simulation, one end of an 801-segment polymer chain was fixed in the center of a sphere with a constant potential of -5.708 eV and with a radius of 2.5 Å, which represents the ruthenium pentaamine coordinated to the ϵ2-nitrogen of His[12]. The other end of the chain was fixed in the center of an ellipsoid with a constant potential of -4.1 eV, which represents the heme. The semimajor axis of the heme is 4.85 Å and the semiminor axis is 2.55 Å; this yields a ground state energy for the isolated ellipsoid of -2.5 eV (*30*), which is the same as the ground state energy for the ruthenium sphere. The potential in the intervening region was evaluated prior to the Monte Carlo on a spatial grid (10 by 10 by 30 Å) with 0.1 Å spacing. The reference potential was featureless (0

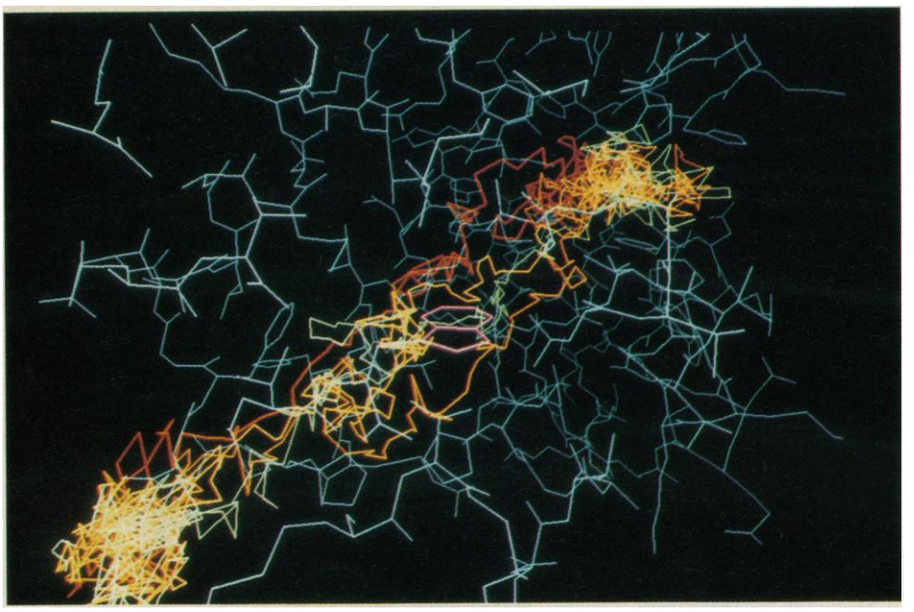

Fig. 1. Four quantum paths for the tunneling electron are depicted (red, yellow, orange, and green) that were sampled from the 500,000 paths of the Monte Carlo run (at $\lambda = 1$). The protein is in light blue with Trp^{14} highlighted in magenta. The heme and ruthenium redox centers are separated by 28.2 Å center-to-center, or 22 Å edge-to-edge.

eV) everywhere except for the wells. The Monte Carlo was performed with the isomorphic polymer chain immersed in the 1217 atom potential at values for the charging parameter λ of 0, 0.02, 0.2, 0.4, and 1.0. The run with $\lambda = 1.0$ corresponds to the fully structured potential. The large repulsive spikes at the core of each atom were troublesome for very low λ but the repulsive spikes could be truncated at a radius of 0.6 Å from the center of each atom with no effect on the polymer chain. The potential of the repulsive core plateau ranged from 78.1 eV to 1495 eV for the various atoms. The code was written in vector form by moving every other bead in the polymer chain, accepting or rejecting the moves, and then moving the other half of the beads. Normal mode moves were tried but this gave a much poorer sampling. 500,000 Monte Carlo moves of the entire polymer were performed for each value of λ and statistics were computed after the initial equilibration period of 100,000 passes.

The ratios of $\Delta(\lambda_2)/\Delta(\lambda_1)$ were computed by evaluating the right-hand side of Eq. 10 and these partial ratios were multiplied together to yield the total ratio $\Delta(\lambda = 1)/\Delta(\lambda = 0)$. We found that increasing β beyond the value used in the simulation ($\beta\hbar = 20$ fsec) had no effect on the structure of the tunneling paths.

Results and discussion. Typical paths of the tunneling electron in the protein are shown in Fig. 1. The individual paths meander considerably but the overall bundle of paths follows a rather direct line from the heme well into the ruthenium well. The overall straightness of the paths must depend upon the balance between attractive regions of the potential that lie off the straight-line path and the "tension" of the harmonic springs in the polymer. This tension, or in the imaginary time perspective, the velocity of the electron, is self-adjusting in the Monte Carlo simulation so long as the total β is sufficiently long. The deeper the energies of the terminal wells, the more the polymer chain will spill into the wells and the higher the tension will be. Hence, the higher the tunneling barrier, the straighter the tunneling paths will be. The imaginary time spent by the electron in the tunneling region (the "kink" or

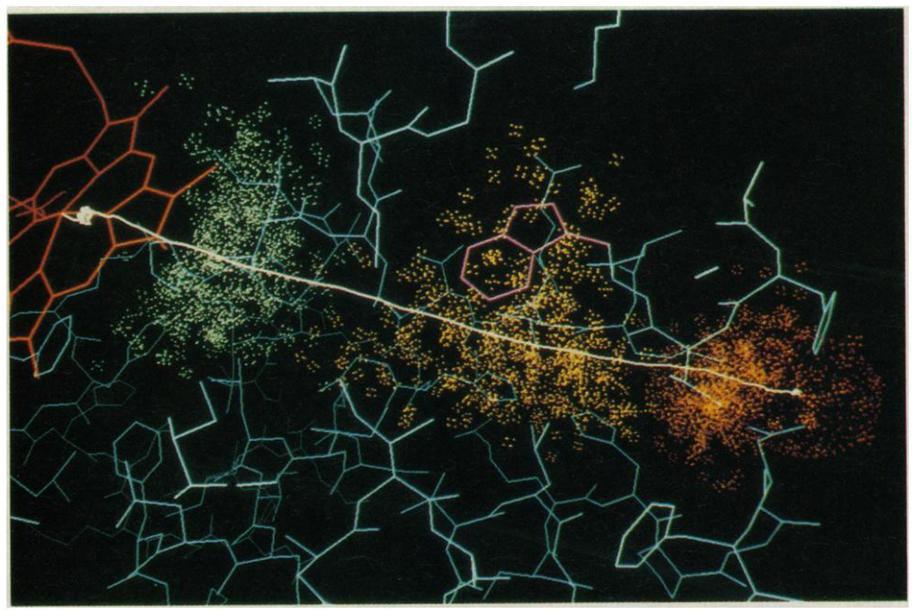

Fig. 2. Dot cloud representation of three time slices of electron tunneling probability density $\rho_{kink}(r)$. The green, yellow, and orange clouds are the first, the tenth, and the nineteenth time slice out of total of 20. Trp^{14} is in magenta. If all the time slices were shown a continuous cylinder would result. This cylindrical zone of electron density defines the region important in controlling the electron tunneling interaction.

"instanton") averaged 2.57 fsec in the full potential runs ($\lambda = 1$) out of a total of 20.0 fsec for the entire path. This is quite near the semiclassical estimate of 2.35 fsec for a one-dimensional barrier that is 22 Å long and 2.5 eV high.

At low values of the charging parameter λ the paths sample the repulsive core regions and the average potential experienced by the tunneling path is positive: +12.4 eV for $\lambda = 0$ and +7.1 eV for $\lambda = 0.02$. The protein overall appears repulsive relative to free space so that the free energy of the kink F_k increases and the tunneling splitting Δ decreases. However, the Monte Carlo paths sampled from the distribution with $\lambda = 0.4$ or greater avoid the atomic cores and thread their way through the attractive regions between the cores; for $\lambda = 1$ the average potential is −1.1 eV. Thus F_k decreases and Δ increases. The final value for the ratio of the tunneling splitting to the reference tunneling splitting is 0.56 ± 0.03 (*31*). This result means that the impediment to tunneling produced by the repulsive cores which restrict the space available to the paths more than offsets the stabilization of the tunneling electron by the attractive regions of the potential. These pictures suggest that optimization of electron tunneling could be achieved by appropriate placement of attractive cavities in the protein.

Shown in magenta in Figs. 1 and 2 is the aromatic ring of Trp^{14}, which has been previously identified as occurring in the through-space line-of-flight of the electron (*32*). We can combine our path results and the linear action relationship to identify precisely the relevant zone of the protein interior responsible for the mediation of the tunneling interaction. The 40,000 independent points (x, y, z, β') along the tunneling section of the paths for $\lambda = 1$ were sorted according to imaginary time β' into "time slices." Three of these time slices are depicted in Fig. 2. These time slices are much like dot-population images of bound-state orbitals and indicate the probability that a given region of space will be visited by the tunneling electron. A loose, discernible cloud of electron probability in the middle time slice surrounds Trp^{14} but it is not a major distortion of this time slice. Trp^{14} does not act as the center of a loosely bound anionic state in our model but quantitation of its role in altering the tunneling splitting must await further comparison calculations.

All of the time slices together define a continuous cylindrical zone that stretches from the heme to the ruthenium with a root-mean-square radius of 1.9 Å. Most time slices are circular in cross section; the greatest axial ratio is 4:3. The center white line in Fig. 2, which is the average path, is fairly straight and has a maximum deviation of 1 Å from the exact center-to-center straight line. Outside of this cylindrical zone only an exponentially small influence of the specific amino acids present upon the tunneling interaction is observed.

In summary, the path integral approach to electron tunneling in proteins provides a method for evaluating the effect of a highly structured intervening medium upon the tunneling interaction. In addition, the linear action relationship (through Eqs. 11 and 12) yields a direct interpretation of the density of electron paths in a region of space as a weighting function for the importance of that region in controlling the tunneling interaction. The methodology introduced here may also be useful in the interpretation of scanning tunneling microscopic studies of biological materials (*33*). Indeed, such experiments may provide one of the best tools for calibrating pseudopotentials in our approach.

REFERENCES AND NOTES

1. B. Chance *et al.*, Eds., *Tunneling in Biological Systems* (Academic Press, New York, 1979).
2. M. Redi and J. J. Hopfield, *J. Chem. Phys.* **72**, 6651 (1980).
3. R. Dickerson, *Sci. Am.* **226**, 58 (April 1972).
4. S. L. Mayo, W. R. Ellis, Jr., R. J. Crutchley, H. B. Gray, *Science* **233**, 948 (1986).
5. N. Liang, G. J. Pielak, A. G. Mauk, M. Smith, B. M. Hoffman, *Proc. Natl. Acad. Sci. U.S.A.*, in press.
6. W. H. Miller, *Science* **233**, 171 (1986).
7. D. Chandler and P. G. Wolynes, *J. Chem. Phys.* **74**, 4078 (1981).
8. S. Coleman, lectures delivered at the 1977 International School of Subnuclear Physics, Ettore Majorana, Erice, in *The Whys of Subnuclear Physics* (Plenum, New York, 1969), p. 805.
9. J. P. Sethna, *Phys. Rev. B* **24**, 698 (1981); *ibid.* **25**, 5050 (1982).
10. L. Szasz, *Pseudopotential Theory of Atoms and Molecules* (Wiley, New York, 1985).
11. D. N. Beratan and J. J. Hopfield, *J. Chem. Phys.* **81**, 5753 (1984).
12. V. G. Levich, *Adv. Electrochem. Electrochem. Eng.* **4**, 249 (1966).
13. H. Frauenfelder and P. G. Wolynes, *Science* **229**, 337 (1985).
14. D. Chandler, K. S. Schweizer, P. G. Wolynes, *Phys. Rev. Lett.* **49**, 110 (1982).
15. D. Thirumalai and B. Berne, *J. Chem. Phys.* **79**, 5029 (1983).
16. K. Binder, *Applications of the Monte Carlo Method in Statistical Mechanics* (Springer-Verlag, New York, 1984).
17. N. Metropolis, A. W. Rosenbluth, M. N. Rosenbluth, A. H. Teller, E. Teller, *J. Chem. Phys.* **21**, 1087 (1953).
18. S. Kirkpatrick, *Disordered Systems and Localization* (Springer-Verlag, Berlin, 1981).
19. B. Widom, *J. Chem. Phys.* **39**, 2808 (1963).
20. P. R. Wells, *Linear Free Energy Relationships* (Academic Press, London, 1968).
21. A. R. Fersht, R. J. Leatherbarrow, T. N. C. Wells, *Nature (London)* **322**, 284 (1986).
22. J. A. McCammon, P. G. Wolynes, M. Karplus, *Biochemistry* **18**, 927 (1979).
23. J. Lekner, *Phys. Rev.* **158**, 130 (1967).
24. The values of r_{vdw} and the polarizability α were taken from the appendix in (*29*) and the extended atom types were classified exactly as described therein. In the case of an atom with zero partial charge the penetration of the excess electron into the core results in $V_{coul} = -(z/r)(1 + \gamma r/2)\exp(-\gamma r)$, where $\gamma = 9.51/r_{vdw}$. The charge-induced dipole energy V_{pol} equals $-\alpha/[2(r^2 + r_{vdw}^2)^{-2}]$. The wave function ψ_{loc}, which is used to convert V_{ex} and V_r into the approximate local forms, is described by the tunneling form $[4/\sinh(4)]\,[\sinh(kr)]/kr$ in the core penetration region and turned over smoothly at $kr = 4$ to the asymptotic value of one. The definite integrals in V_{ex} and V_r containing ψ_e and ψ_{loc} were written in γ-independent form and integrated numerically. The sum over atoms in Eq. 13 was then evaluated on a spatial grid.
25. N. R. Kestner, J. Jortner, M. H. Cohen, S. A. Rice, *Phys. Rev.* **140**, A56 (1965).
26. M. H. Cohen and V. Heine, *ibid.* **122**, 1821 (1961).
27. N. F. Mott and H. S. W. Massey, *The Theory of Atomic Collisions* (Oxford Univ. Press, New York, ed. 3, 1965).
28. R. Schiller, Sz. Vass, J. Mandics, *Int. J. Radiat. Phys. Chem.* **5**, 491 (1973).
29. S. H. Northrup, M. R. Pear, J. D. Morgan, J. A. McCammon, M. Karplus, *J. Mol. Biol.* **153**, 1087 (1981).
30. P. Siders, R. J. Cave, R. A. Marcus, *J. Chem. Phys.* **81**, 5613 (1984).
31. The error quoted is the standard deviation of the mean. Calculations of

$$\langle \exp[-(\lambda_2 - \lambda_1)(\beta/P) \sum_i V(x_i)] \rangle_{\lambda_1}$$

and

$$\langle \exp[-(\lambda_1 - \lambda_2)(\beta/P) \sum_i V(x_i)] \rangle_{\lambda_2}^{-1}$$

gave the same values to within 3%.
32. R. A. Scott, A. G. Mauk, H. B. Gray, *J. Chem. Ed.* **62**, 932 (1986).
33. A. M. Baro *et al.*, *Nature (London)* **315**, 253 (1985).

34. We thank R. A. Scott, R. W. Hall, J. J. Hopfield, and R. A. Marcus for helpful discussions while this work was in progress. The support from the National Science Foundation, the ACS Petroleum Research Fund, and an NIH postdoctoral fellowship F32 GM10211 to A.K. are acknowledged. We also thank the National Center for Supercomputing Applications and the NSF Office of Advanced Scientific Computing for the grant of time and their cooperation.

21 January 1987; accepted 20 May 1987